Uptake of ^{18}F-fluorocholine, ^{18}F-fluoro-ethyl-L-tyrosine and ^{18}F-fluoro-2-deoxyglucose in F98 gliomas in the rat

Nicolas Spaeth[1], Matthias T. Wyss[1,2], Jens Pahnke[3], Gregoire Biollaz[4], Amelie Lutz[5], Kerstin Goepfert[5], Gerrit Westera[2], Valerie Treyer[1], Bruno Weber[1], Alfred Buck[1]

[1] PET Center, Division of Nuclear Medicine, University Hospital, Rämistrasse 100, 8091 Zürich, Switzerland
[2] Center for Radiopharmaceutical Science of ETH, PSI and USZ, Paul Scherrer Institute, Villigen und University Hospital Zurich, Zurich, Switzerland
[3] Department of Pathology, University Hospital Zurich, Zurich, Switzerland
[4] Section of Clinical Immunology, University Hospital Zurich, Zurich, Switzerland
[5] Institute of Diagnostic Radiology, University Hospital Zurich, Zurich, Switzerland

Received: 18 July 2005 / Accepted: 16 November 2005 / Published online: 15 March 2006

Abstract. *Introduction:* The positron emission tomography (PET) tracers ^{18}F-fluoro-ethyl-L-tyrosine (FET), ^{18}F-fluorocholine (*N*,*N*-dimethyl-*N*-[^{18}F]fluoromethyl-2-hydroxyethylammonium (FCH]) and ^{18}F-fluoro-2-deoxyglucose (FDG) are used in the diagnosis of brain tumours. The aim of this study was threefold: (a) to assess the uptake of the different tracers in the F98 rat glioma, (b) to evaluate the impact of blood-brain barrier (BBB) disruption and microvessel density (MVD) on tracer uptake and (c) to compare the uptake in the tumours to that in the radiation injuries (induced by proton irradiation of healthy rats) of our previous study.
Methods: F98 gliomas were induced in 26 rats. The uptake of FET, FCH and FDG was measured using autoradiography and correlated with histology, disruption of the BBB and MVD.
Results: The mean FET, FCH and FDG standardised uptake values (SUVs) in the tumour and the contralateral normal cortex (in parentheses) were 4.19±0.86 (1.32± 0.26), 2.98± 0.58 (0.51±0.11) and 11.02±3.84 (4.76±1.77) respectively. MVD was significantly correlated only with FCH uptake. There was a trend towards a negative correlation between the degree of BBB disruption and FCH uptake and a trend towards a positive correlation with FET uptake. The ratio of the uptake in tumours to that in the radiation injuries was 1.97 (FCH), 2.71 (FET) and 2.37 (FDG).
Conclusion: MVD displayed a significant effect only on FCH uptake. The degree of BBB disruption seems to affect the accumulation of FET and FCH, but not FDG. Mean tumour uptake for all tracers was significantly higher than the accumulation in radiation injuries.

Alfred Buck (✉)
Nuclear Medicine,
University Hospital,
Rämistrasse 100,
8091 Zürich, Switzerland
e-mail: fred.buck@usz.ch
Tel.: +41-125-53547, Fax: +41-125-54414

Keywords: F98 glioma – ^{18}F-fluorocholine – ^{18}F-fluoro-ethyl-L-tyrosine – ^{18}F-fluoro-2-deoxyglucose – Autoradiography

Eur J Nucl Med Mol Imaging (2006) 33:673–682
DOI 10.1007/s00259-005-0045-7

Introduction

Positron emission tomography (PET) is a well-established modality in the evaluation of brain tumour patients. Twenty-two years ago the first brain tumour images were acquired with ^{18}F-fluoro-2-deoxyglucose (FDG), which has become the most widely used tracer in PET imaging [1]. Although the usefulness of FDG in tumour imaging is beyond doubt, there are drawbacks. The high physiological uptake in the brain often renders it difficult to differentiate tumour from normal brain tissue, a problem which cannot always be overcome by correlation with structural imaging. Another problem is the large range of FDG uptake in different brain tumours, leading to an overlap with the degree of uptake in benign lesions [2, 3]. Furthermore, FDG is taken up by tumour cells as well as inflammatory cells, reducing its specificity in oncological imaging [4, 5].

These limitations led to the development of new radiotracers such as radiolabelled choline compounds (e.g. ^{18}F-fluorocholine: *N*,*N*-dimethyl-*N*-[^{18}F]fluoromethyl-2-hydroxy-ethylammonium [FCH]) or amino acid analogues like ^{18}F-fluoro-ethyl-L-tyrosine (FET). Both tracers show a high tumour to background ratio, which facilitates the detection and delineation of especially low-grade and/or cortical tumours. They also seem promising candidates for the differentiation of recurrent brain tumour from radiation injury [6–8]. Moreover, FET, unlike FCH and FDG, does not accumulate in inflammatory cells, a feature which increases the specificity of FET in tumour imaging [9–11].

FET is an amino acid analogue which is not metabolised or incorporated into proteins [12]. A specific Na^+-independent amino acid transport system, the L-system, as well as the Na^+-dependent system $B^{0,+}$, is responsible for the high FET accumulation in different tumour cell lines [13, 14]. Wester et al. introduced this tracer to clinical research [12]. Further studies have demonstrated an increased uptake of FET in various brain tumours [8, 15–18], but there are still open questions concerning the main uptake mechanism(s) of FET in vivo. Besides the L- and $B^{0,+}$ systems, which are located in the membranes of brain endothelial cells (L) and tumour cells (L, $B^{0,+}$), blood-brain barrier (BBB) disruption, tumour perfusion and the microvessel density (MVD) could influence tracer accumulation. In this respect, Kracht et al. found a positive correlation between the microvessel count and the uptake of [^{11}C]methionine (MET), a radiolabelled amino acid widely used as a tracer in gliomas [19]. To our knowledge no data are available on the correlation between the MVD and FET uptake.

Choline, an important compound of the cell membrane, is transported into mammalian cells by a low-affinity sodium-independent transport system and then phosphorylated by choline kinase [20]. In a further step it is metabolised to phosphatidylcholine, which is incorporated into the cell membrane. In previous studies the increased choline uptake in tumour cells was mainly explained by the upregulation of choline kinase due to an increased demand of membrane constituents [21–23]. However, Henriksen et al. postulated a specific choline transport system in tumour cells as the major mechanism for the clinically important early uptake of radiolabelled choline derivatives [24]. Initial clinical studies with [^{11}C]choline demonstrated the diagnostic potential of this substance in different tumours [25–29]. DeGrado et al. introduced FCH for brain tumour imaging [30]. The major advantage of ^{18}F-labelled compounds, especially in clinical use, is the longer physical half-life of ^{18}F (110 min) compared with ^{11}C (20 min). This allows several PET examinations with one production. The tumour uptake pattern of [^{11}C]choline and ^{18}F-substituted choline analogues is very similar [7]. As mentioned above, tumour uptake seems highly related to transport and choline kinase activity of the tumour cells themselves but can also be influenced by the BBB (specific transport or disruption), tumour perfusion and the MVD.

The aim of this study was threefold: (a) to assess the uptake of the different tracers in the F98 rat glioma, (b) to evaluate the impact of BBB disruption and MVD on tracer uptake and (c) to compare the uptake in the tumours to that in the radiation injuries of our previous study [31]. In that project, radiation injuries were induced with 150 or 250 Gy proton irradiation. Following the development of a circumscribed lesion, the uptake of FET, FCH or FDG was measured using autoradiography and correlated with the histology and the disruption of the BBB.

Materials and methods

Animals

A total of 26 male Fischer 344 rats weighing 250–300 g were used in this study. The experiments were approved by the local veterinary authorities of the Canton of Zurich/Switzerland.

Radiopharmaceuticals

FDG was obtained from the commercial FDG production of the University Hospital Zurich. The production of FET and FCH has been described in detail elsewhere [31].

Cell culture

The rat glioma cell line F98 was provided by G. Mies (Cologne, Germany). F98 cells were grown in DMEM containing 4,500 mg/l D-glucose (GIBCO, Life Technologies, Basel, Switzerland) supplemented with 10% FCS, 2 m*M* *N*-acetyl-L-alanyl-L-glutamine (Biochrom AG, Germany) and 20 μg/ml gentamicin (Sigma-Aldrich, Germany). For injection, cells were harvested by trypsinisation, washed 3 times with PBS and resuspended at a final concentration of 50 million cells/ml.

Inoculation procedure

Rats were anaesthetised with an intraperitoneal injection of a ketamine (100 mg/kg; Ketasol 100, Dr. E. Graeub AG, Bern, Switzerland)/xylazine (10 mg/kg; Xylasol, Dr. E. Graeub AG, Bern, Switzerland) mixture and placed in a stereotactic frame. We used the inoculation method of Ambar et al. with minor modifications [32]. After preparation of the inoculation area, a small hole was drilled into the skull. Then, 1×10^6 F98 cells in 2 μl were implanted into the left parietal cortex at a depth of 1 mm ventral to the dura mater using a 10 μl–26 gauge Hamilton syringe (Hamilton, Bonaduz, Switzerland). After a short incubation time the syringe was slowly removed and the hole was closed. The well-being of the animals were then monitored daily.

Magnetic resonance imaging

Every second rat was examined once with MRI between day 7–14 after inoculation for tumour growth control. Magnetic resonance imaging (MRI) was performed on a 1.5-T system (GE Signa EchoSpeed Plus 1.5 T with Excite II, GE Healthcare, WI, USA). To maximise the signal to noise ratio, animals were positioned in a dedicated wrist coil. The imaging protocol included the following sequences: an unenhanced transaxial T1-weighted spin echo (SE) sequence [repetition time (TR)/echo time (TE)=300 ms/13 ms; slice thickness 3 mm, without an interslice gap] and a transaxial or coronal T2-weighted three-dimensional (3D) fast SE sequence (FSE) (TR/T 3,000/128, slice thickness 1.5 mm). In addition, the T1-weighted sequence was acquired in the transaxial or coronal plane following intravenous administration of gadopentetate dimeglumine (Gd-DPTA; Magnevist, Schering AG, Berlin, Germany; 0.1 mmol/kg body weight) via a tail vein.

Autoradiography with FET, FCH and FDG

After detection of a tumour on MRI scans, autoradiography was performed (9–23 days after inoculation). Under isoflurane inhalation anaesthesia, catheters were placed in the right femoral artery to monitor blood pressure and the femoral vein to allow intravenous administration of the tracers and Evans Blue, which was injected 1 h prior to tracer administration. Evans Blue binds to albumin and therefore acts as an intravascular contrast medium. More information is given in the next section. According to basic biodistribution studies, 15 min (FCH [33] and FET [8]) and 45 min (FDG [34]) were chosen as tracer uptake times. Following injection of 100–150 MBq of tracer, the animals were sacrificed using an overdose of pentobarbital. The brain was removed and instantly frozen in cooled isopentane. For quantification, 10-µm brain slices (100-µm slice distance) were placed on a phosphor imaging screen together with ^{14}C standards and left for 240 min. Tritium-sensitive screens (Fuji TR2025) were used as their uncoated, thin, sensitive layer yields higher resolution ^{18}F autoradiographs than ordinary screens. The data were scanned (Fuji BAS 1800 II, pixel size 50 µm) and converted to kBq/cc. For this conversion the ^{14}C standards had previously been recalibrated using the data of a 4-h exposure of 10-µm slices of a brain homogenate containing a defined amount of ^{18}F activity.

For quantitative analysis the activities were then decay corrected to the time of injection. Dividing these values by the amount of injected activity per gram of body weight yielded standardised uptake values (SUVs). Regions of interest (ROIs) were subsequently placed over the area of average tracer uptake in the tumours and over the contralateral healthy cortex using the software PMOD [35]. The division of tumour by contralateral cortex SUVs revealed tumour to normal brain ratios (TBRs).

Morphological characterisation

For morphological analysis the brains were taken and fixed in 4% formalin/PBS, followed by haematoxylin/eosin (H&E) conventional stain and GFAP (glial fibrillary acidic protein) immunohistochemistry. Briefly, slides were incubated with anti-GFAP antibody (1:1,000, DAKO Z0334) without pretreatment. Slides were then developed using a Ventana machine and the iView DAB (DAKO) development kit.

For histological analysis of the MVD and the BBB leakage, brains were frozen in isopentane cooled to −50°C. For the visualisation of Evans Blue, 10-µm thick slices were fixed with formalin 4% and stained with DAPI (molecular probes, D-1306).

In each animal the Evans Blue distribution was evaluated on one typical slice through the tumour. For this purpose the sections were investigated in a fluorescence microscope (Leica MZ16 FA, Leica Microsystems AG, Wetzlar, Germany) with the following filter combination: excitation 540–580 nm, emission 610 nm low pass. The data were stored as an 8 bit intensity image. ROIs were then placed on the tumour and the contralateral cortex, and the mean of the ROI was taken as a measure for relative fluorescence intensity. As was demonstrated in the work by Saria and Lundberg [36], this intensity is linearly correlated with the absolute density of Evans blue. The ratio of the fluorescence intensity in tumour and contralateral cortex was taken as a measure of BBB disruption, which was then correlated with the SUV of tracer uptake.

The MVD was assessed in 22 rats using the von Willebrandt factor stain (vWF). Briefly, brain slices were pretreated with protease 1 for 4 min and stained with polyclonal antibody against vWF (1:1,000, DAKO A00802). The staining was developed using iVIEW DAB (DAKO). The number of vessels was counted in a totally visible tumour diameter of one representative section according to Weidner et al. [37]. For comparison, the counts were then adjusted to number per 10 microscopic high-power fields (0.1885 mm^2 per HPF).

Statistics

The present tumour data were compared with those regarding radiation injury from our previous study [31]. The combined data were analysed using a two-way analysis of variance with type of lesion (tumour, radiation injury) and type of tracer (FCH, FET, FDG) as factors. Spearman rank correlation analyses were performed between tracer uptake in tumour tissue (quantified as SUV and TBR) and both microvessel density (MVD) and extravasation of Evans Blue (EB). Owing to the relatively small number of animals, the calculated *p* values were not corrected for multiple comparisons.

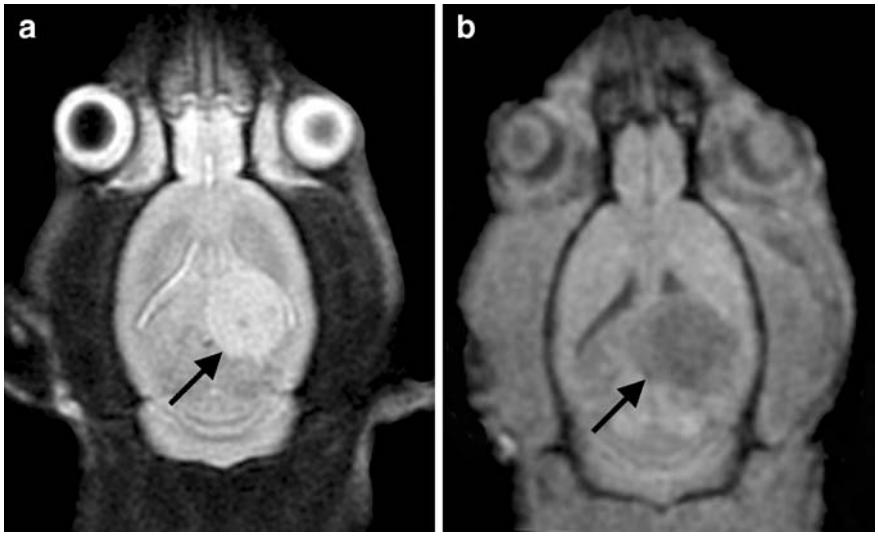

Fig. 1. The axial MRI scans of the rat brain clearly depict the F98 glioma in the left temporoparietal cortex. On the T2-weighted three-dimensional fast SE sequence the tumour demonstrates increased signal intensity (**a**, *arrow*). On the T1-weighted SE scan the signal intensity is decreased (**b**, *arrow*)

Results

Animals

No animal suffered from systemic side-effects during the period of observation, except for two rats which developed neurological signs. These animals were immediately euthanised.

Development of the F98 glioma

Intracerebral lesions were detected on the MRI scans 7–14 days after inoculation. The diameter of the tumour ranged from 3 to 6 mm. Typical examples of MRI scans are demonstrated in Fig. 1. The tumour was located within the cortex of the left temporo-parietal region and extended into the white matter.

Morphological characterisation

Histological slices of a typical F98 glioma infiltration are shown in Fig. 2. The glioma cells diffusely infiltrate the surrounding brain parenchyma. Occasionally, tumour cells formed round and expanding cell bulks. Atypical mitosis were often seen.

Disruption of the blood-brain barrier

Typical examples of Evans Blue fluorescent scans are illustrated in the left panels of Fig. 3. Extravasation of Evans Blue as an indication of BBB disruption was present in each case.

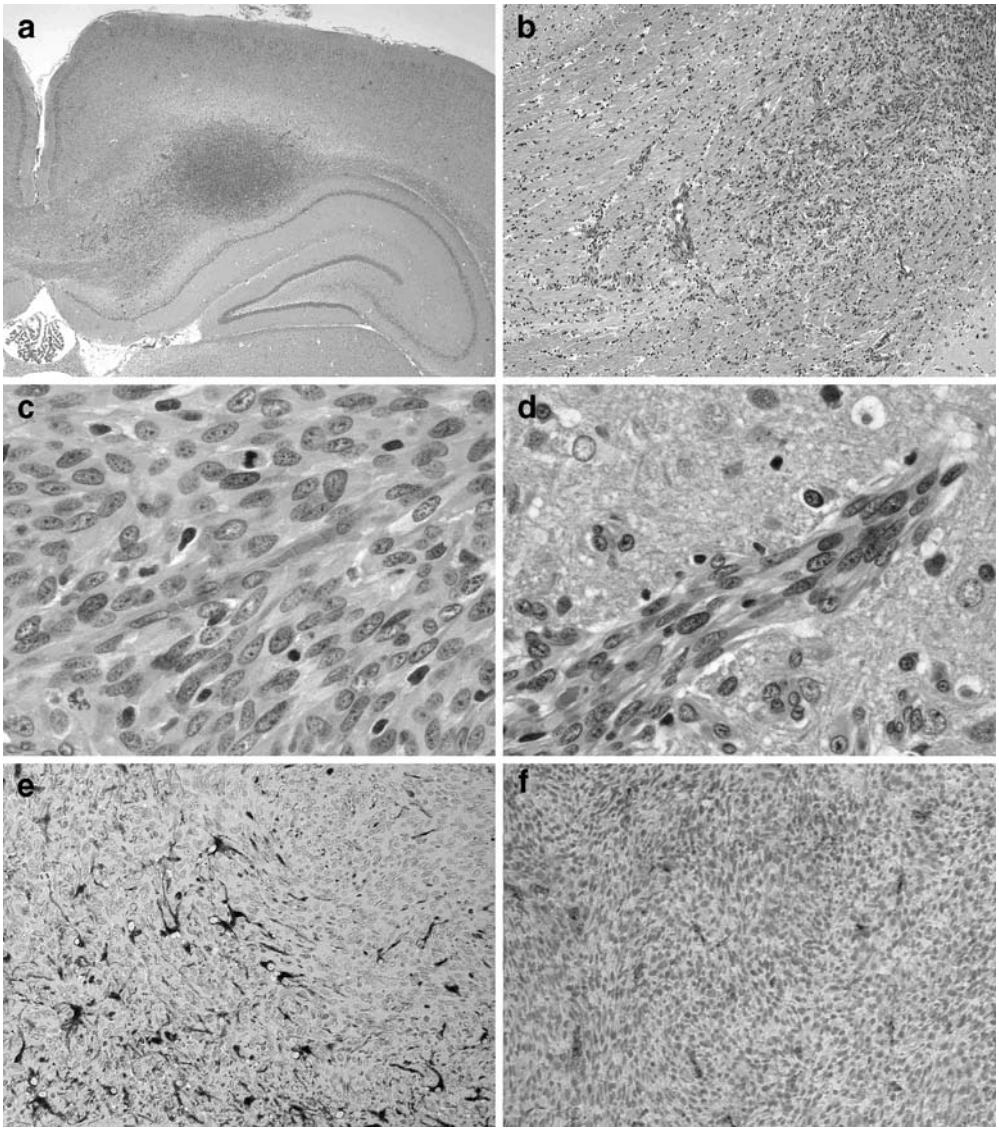

Fig. 2. Microscopic images of F98 glioma cell transplants in rat brains. **a** The side of transplantation in the left hemisphere near the corpus callosum (H&E, ×1.625). **b** Higher magnification of the infiltration zone of the F98 glioma cells (H&E, ×40). **c** Tumour microvessel (*centre*) filled with erythrocytes (H&E, ×400). **d** The perivascular infiltration of the tumour cells (H&E, ×400). Cells spread along microvessels in the Virchow-Robin perivascular space. **e** Immunohistochemically labelled host astrocytes and F98 glioma cells (anti-GFAP, ×100). As in human glioblastoma, F98 glioma transplants show only occasional positivity for GFAP. **f** Anti-vWF labelled microvessels within the F98 glioma transplant (anti-vWF, ×200)

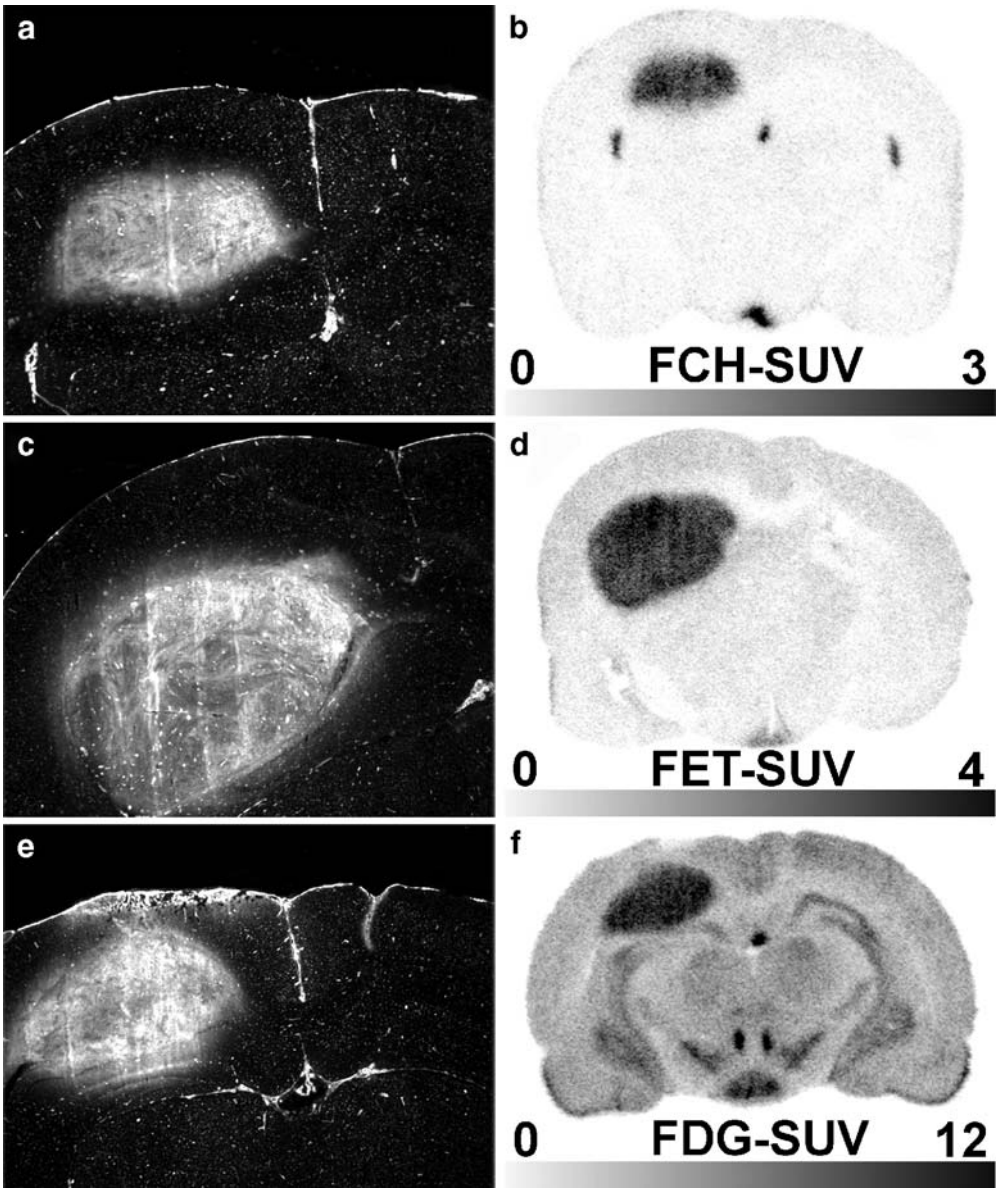

Fig. 3. The *left side of the figure* (**a, c, e**) depicts the disruption of the BBB as demonstrated by the leakage of Evans Blue. The uptake of FCH (**b**), FET (**d**) and FDG (**f**) is shown on the *right*

Microvessel density

Transplanted tumour cells exhibit a homogeneous tumour mass with a fine network of small arterioles and capillaries. A representative section of the tumour mass shows an evenly distributed microvascular network (Fig. 2f). Summarising, the mean vessel count in the total sample of 22 histologically analysed rats was 179±59 (mean±standard deviation) per 10 HPFs (0.1885 mm^2 per HPF).

Tracer uptake and correlation with the extravasation of Evans Blue, microvessel density and uptake in radiation injury

Examples of autoradiographs of each tracer are demonstrated on the right side of Fig. 3. Each tumour displayed markedly higher tracer uptake than the surrounding tissue. The uptake values are summarised in the left part of Table 1. For comparison the corresponding values in the radiation injuries of our previous study [31] are presented on the right of Table 1 and illustrated in Fig. 4. FDG displayed the highest SUV, followed by FET and FCH. The tumour/cortex ratio was highest for FCH. In the tumours the mean SUV was 1.97 (FCH), 2.71 (FET) and 2.37 (FDG) times higher than in the radiation injuries. For FET there was no overlap of the SUV in the tumour and radiation injury, while for FCH and FDG the tumour SUV was in the same range as the uptake in the radiation injury in only one animal. For the lesion to cortex ratio there was no overlap at all. The analysis of variance performed on the SUV data demonstrated significant main effects of lesion type ($F_{(1,39)}$=45.71, p<0.001) and type of tracer ($F_{(2,39)}$=25.42; p<0.001) as well as a significant interaction between the two ($F_{(2,39)}$=8.03; p<0.005). It is important to

note that the methodology for the derivation of the SUVs was the same in the gliomas and the radiation injuries.

The correlation of tracer uptake (SUV, TBR), MVD and extravasation of Evans Blue (EB) is demonstrated in Fig. 5. A significant positive correlation was found between relative uptake of FCH and MVD. The same tracer demonstrated a trend towards a negative correlation between uptake and extravasation of Evans Blue. Another trend towards a relevant correlation was present for FET SUV and extravasation of Evans Blue.

No correlation was found between MVD and extravasation of Evans Blue (data not shown).

Table 1. SUVs of F98 gliomas and radiation injury

Tracer	Animal	F98 glioma		Animal	Radiation injury	
		Tumour	Tumour/CTX		Nec	Nec/RTX
FCH	1	3.21	6.42	1	1.38	2.38
FCH	2	2.83	5.90	2	1.43	2.65
FCH	3	3.01	7.34	3	1.43	2.70
FCH	4	1.93	3.64	4	1.12	2.07
FCH	5	4.08	5.59	5	1.25	2.12
FCH	6	3.03	5.41	6	1.99	3.32
FCH	7	2.92	5.73	7	1.92	2.23
FCH	8	3.04	9.50			
FCH	9	2.73	4.79			
Mean		2.98	6.03		1.50	2.50
SD		0.58	1.65		0.33	0.44
FET	1	3.98	3.24	1	0.90	1.23
FET	2	2.88	2.46	2	1.29	1.08
FET	3	4.60	3.26	3	1.39	0.89
FET	4	4.21	4.13	4	1.82	1.07
FET	5	5.07	2.93	5	1.80	1.42
FET	6	4.91	3.13	6	1.92	1.78
FET	7	3.47	3.15	7	1.52	0.97
FET				8	1.69	1.10
Mean		4.19	3.19		1.54	1.19
SD		0.86	0.50		0.34	0.29
FDG	1	5.21	1.43	1	3.66	0.85
FDG	2	10.68	1.83	2	4.35	1.20
FDG	3	17.03	1.96	3	4.48	1.02
FDG	4	9.22	2.85	4	5.28	1.04
FDG	5	9.67	2.61	5	3.93	0.93
FDG	6	15.91	3.38	6	6.11	1.37
FDG	7	8.99	2.22			
FDG	8	11.42	2.71			
Mean		11.02	2.37		4.64	1.07
SD		3.84	0.63		0.91	0.19

FCH^{18} F-*N*, *N*-dimethyl-*N*-[^{18} F]fluoromethyl-2-hydroxy-ethylammonium, *FET*^{18} F-fluoro-ethyl-L-tyrosine, *FDG*^{18} F-fluoro-2-deoxyglucose, *SUV* standardised uptake value, *Tumour* average SUV in the area of the F98 glioma, *Nec* average SUV in the area of the radiation necrosis, *CTX* contralateral cortex

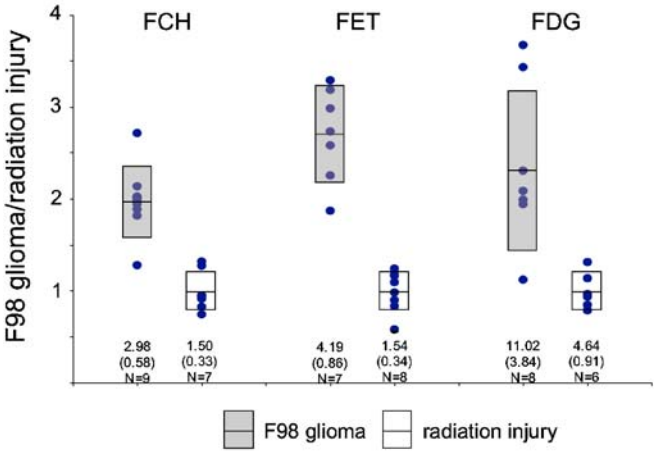

Fig. 4. Comparison of tracer uptake in F98 glioma and in radiation injuries from a previous study. For the presentation the data were normalised to the mean of the uptake in the radiation injuries. The data points represent individual animals. The *bars* are centered on the mean and represent ±1SD. The numbers signify the mean SUV of the original data and the coefficient of variation (SD/mean×100) in percent

Discussion

The F98 rat glioma model proved to be very reliable. Because the tumours have similar characteristics to certain human high-grade brain tumours [38], the results are relevant for the interpretation of human PET scans. For instance, the F98 rat glioma has similar growth characteristics to the glioblastoma multiforme, the most common human primary brain tumour, as is demonstrated in Fig. 2. Furthermore, the cell line is syngeneic in inbred Fischer rats, which leads to a negligible immune response. This is important because tumour uptake is not confounded by uptake into activated inflammatory cells.

Tumour uptake of the different tracers

Not unexpectedly, FDG displayed the highest tumour SUV of all tracers. The lowest SUV was measured with FCH. Although it must be mentioned that a direct comparison of our data with human studies is limited by various factors, such as different acquisition protocols and modalities as well as interspecies differences, for all tracers the SUVs and TBRs were in the range of those observed in human high-grade gliomas [3, 6, 16, 18, 39]. This correspondence is another indication of the usefulness of the used glioma model.

The second aim of the study was to evaluate the effect of BBB disruption and MVD on tracer uptake. This aim was inspired by another study, where the uptake of [^{11}C] methionine in 21 glioma patients was reported to correlate with MVD [19]. In our study no such correlation was found

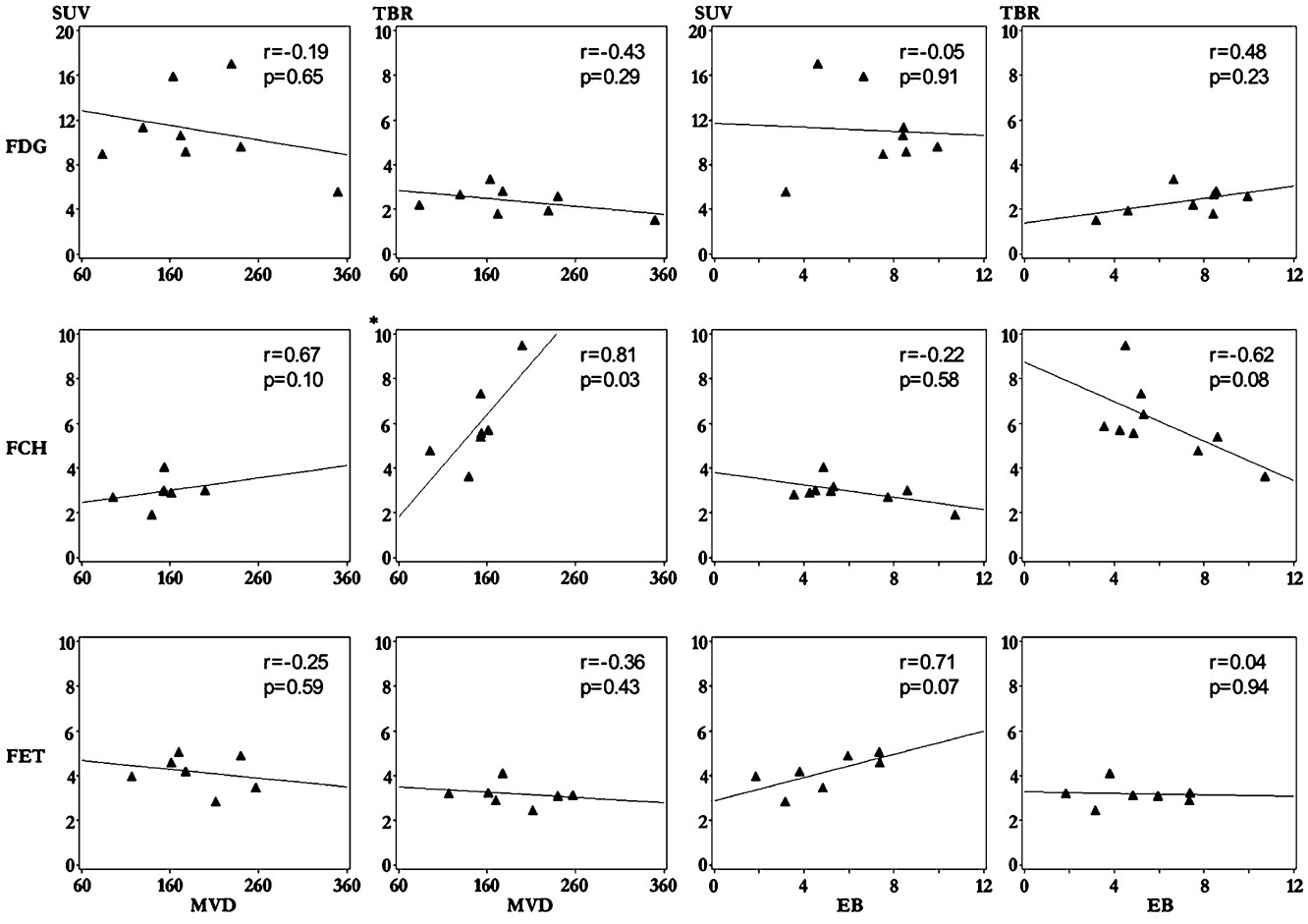

Fig. 5. Correlations between tracer uptake [standardised uptake value (*SUV*) and tumour to normal brain ratio (*TBR*)] and microvessel density (*MVD*) and the extravasation of Evans Blue (*EB*). The *r* values represent Spearman's correlation coefficient

for FET, the amino acid analogue among our investigated tracers. This result suggests that the increased FET uptake in the F98 glioma is mainly determined by a mechanism located in the tumour cells themselves whereas active transport across the BBB into the interstitial space is probably not a rate-limiting factor. Very likely candidates for this mechanism are up-regulated amino acid transporters like system L [L amino acid transporter (LAT) 1–3] and $B^{0,+}$ in the tumour cell membrane [14]. According to previous studies, the LAT2 and $B^{0,+}$ systems seem to be the main FET transporters in F98 glioma cells [14, 40].

In addition, we found a trend towards a positive correlation between FET uptake and the extent of BBB leakage, which almost reached significance. This result is in line with our previous experiments in radiation injuries and cryolesions. These experiments demonstrated that a disruption of the BBB led to considerable leakage of FET into interstitial space [31].

In contrast to FET, a significant correlation between tracer uptake and MVD was found for FCH. This finding is in line with the work by Shinoura et al., which demonstrated that [^{11}C]choline TBRs in brain tumours increased with vessel density [41]. In addition, we found a tendency towards a negative correlation between FCH uptake and extravasation of Evans Blue (Fig. 5). This indicates that the choline carriers which transport FCH across the vessel wall into the interstitial space are a relevant factor in the kinetic chain determining FCH uptake [6, 42]. A higher degree of BBB disruption is probably associated with less function of the choline carriers in the vessel wall, which might explain the lower FCH uptake with increasing BBB disruption. A possible passive leakage of FCH across a disrupted BBB does not seem to compensate for the decreased function of the choline carriers in tumour vessels. The present study does not elucidate the importance of the mechanisms located in the tumour cells for FCH accumulation. However, there is evidence that a choline-specific transport system is primarily responsible for the early uptake of radiolabelled choline analogues in different tumour cell lines [24]. Further studies should also address the role of choline kinase on FCH accumulation using a specific inhibitor like MN58b [43].

For FDG no significant correlation of tracer uptake and MVD or BBB disruption was found. This is in contrast to the human study by Aronen et al. [44]. These authors correlated the FDG uptake in 21 gliomas with microvascular blood volume (TBV) in the tumours measured with MRI. They reported a relevant positive correlation in 16 of

these tumours. The fact that Aronen et al. used different types of glioma may explain the discrepancy with our study. It is known that higher grade of malignancy is often coupled with increased MVD [37, 45]. However, experimental proof is lacking on whether the increased MVD directly leads to higher tracer uptake. It is well possible that an altered mechanism in the malignant cells is responsible for the increased tracer retention and that the higher MVD is coincidental. In fact, our study with a single cell line favours this latter possibility for FDG and FET. For FCH, the MVD seems to play a more direct role in tracer retention. This may be relevant if the tracer is to be used for tumour grading. The potential for such grading has been demonstrated for FDG [1, 46, 47]. Since increased MVD is associated with higher tumour malignancy and seems also to be a factor determining FCH uptake, the latter might in addition be related to tumour malignancy. This possibility should be tested in further studies. In contrast, FET PET does not seem to be a reliable diagnostic tool for grading brain tumours [16, 48–50]. However, this tracer is very suitable for the differentiation of malignant from benign lesions [8, 9, 11, 15, 16, 18].

Comparison of tracer uptake in F98 gliomas and radiation injuries

The differentiation of radiation injury from recurrent tumour is a relevant clinical problem in brain tumour patients who have been irradiated. In our previous study we investigated the uptake of all three tracers in experimentally induced acute radiation injuries in healthy rat brains [31]. The comparison clearly demonstrated that the uptake of all used tracers was significantly higher in the F98 gliomas (Table 1, Fig. 4). For SUV or lesion/contralateral cortex ratios there was no or only minimal overlap between the tumour and the radiation injury group. The significant interaction of lesion type and tracer in the analysis of variance indicates that there is a difference in the ability of the investigated tracers to distinguish tumour from radiation injury. Visual inspection of Fig. 4 reveals that FET seems most favourable. However, FCH and FDG also seem very suitable.

In clinical practice, the situation is more complicated. FDG has several drawbacks in the differentiation of radiation injury from recurrent tumour. For instance, FDG uptake varies over a wide range in different brain tumours, and some low- and even some high-grade tumours display the same or lower FDG SUVs than are measured in acute radiation injuries [3, 39]. Another problem is the high accumulation of FDG in normal brain tissue, which often makes it difficult to identify a lesion.

The situation seems more favourable for FET. In addition to the present study, other publications have indicated that FET PET holds promise for the differentiation of benign therapy-induced lesions from recurrent tumour [8, 16]. Gliomas generally display a higher uptake than benign lesions like radiation injuries.

For FCH the available data on human brain tumours are still very limited. The only available SUV data were published by research groups at the Gunma University School of Medicine, Maebashi, Japan, and the University of Turku in Helsinki, Finland, both using [^{11}C]choline PET [3, 51–53]. The SUV was in the range 0.17–4.40 in different high-grade gliomas and 0.07–3.31 in low-grade gliomas. For comparison, SUVs in non-neoplastic brain lesions (n=5) ranged from 0.17 to 1.22, indicating overlap with the tumours. In contrast, our investigations demonstrated that FCH is a promising tracer for the differentiation of tumour from radiation injury.

In summary, the accumulation of FCH, FET and FDG is highly increased in F98 rat gliomas relative to uptake in normal brain. Higher MVD led to higher FCH uptake while it had no effect on the accumulation of FET or FDG. The degree of BBB disruption seems to influence the accumulation of FET and FCH, but not that of FDG. For all tracers, tumour uptake was significantly higher than the accumulation in radiation injuries, with almost no overlap between the groups. This is important for the differentiation of tumour from radiation injuries in clinical applications.

Acknowledgements. This study was supported by the Sassela-Stiftung, the Olga Mayenfisch-Stiftung and the Huggenberger-Bischof-Stiftung in Zurich. The authors thank Gustav K. von Schulthess and Dominik Weishaupt for valuable discussions, as well as Tibor Cservenyak and Rolf Hesselmann for production of the studied tracers. Valerie Treyer was supported by the Swiss National Science Foundation.

References

1. Di Chiro G, DeLaPaz RL, Brooks RA, Sokoloff L, Kornblith PL, Smith BH, et al. Glucose utilization of cerebral gliomas measured by [^{18}F] fluorodeoxyglucose and positron emission tomography. Neurology 1982;32:1323–1329
2. Ricci PE, Karis JP, Heiserman JE, Fram EK, Bice AN, Drayer BP. Differentiating recurrent tumor from radiation necrosis: time for re-evaluation of positron emission tomography? AJNR Am J Neuroradiol 1998;19:407–413
3. Ohtani T, Kurihara H, Ishiuchi S, Saito N, Oriuchi N, Inoue T, et al. Brain tumour imaging with carbon-11 choline: comparison with FDG PET and gadolinium-enhanced MR imaging. Eur J Nucl Med 2001;28:1664–1670
4. Kaim AH, Weber B, Kurrer M, Gottschalk J, von Schulthess GK, Buck A. Autoradiographic quantification of ^{18}F-FDG uptake in experimental soft tissue abscesses in rats. Radiology 2002;223:446–451
5. Kubota R, Yamada S, Kubota K, Ishiwata K, Tamahashi N, Ido T. Intratumoral distribution of fluorine-18-fluorodeoxyglucose in vivo: high accumulation in macrophages and granulation tissues studied by microautoradiography. J Nucl Med 1992;33:1972–1980
6. Hara T, Kondo T, Kosaka N. Use of ^{18}F-choline and ^{11}C-choline as contrast agents in positron emission tomography imaging-guided stereotactic biopsy sampling of gliomas. J Neurosurg 2003; 99:474–479
7. Hara T. ^{11}C-choline and 2-deoxy-2-[^{18}F]fluoro-D-glucose in tumor imaging with positron emission tomography. Mol Imaging Biol 2002;4:267–273

8. Weber WA, Wester HJ, Grosu AL, Herz M, Dzewas B, Feldmann HJ, et al. *O*-(2-[^{18}F]fluoroethyl)-L-tyrosine and L-[methyl-^{11}C]methionine uptake in brain tumours: initial results of a comparative study. Eur J Nucl Med 2000;27:542–549
9. Kaim AH, Weber B, Kurrer MO, Westera G, Schweitzer A, Gottschalk J, et al. ^{18}F-FDG and ^{18}F-FET uptake in experimental soft tissue infection. Eur J Nucl Med Mol Imaging 2002;29:648–654
10. Wyss MT, Weber B, Honer M, Spath N, Ametamey SM, Westera G, et al. ^{18}F-choline in experimental soft tissue infection assessed with autoradiography and high-resolution PET. Eur J Nucl Med Mol Imaging 2003;20:20
11. Rau FC, Weber WA, Wester HJ, Herz M, Becker I, Kruger A, et al. *O*-(2-[^{18}F]Fluoroethyl)-L-tyrosine (FET): a tracer for differentiation of tumour from inflammation in murine lymph nodes. Eur J Nucl Med Mol Imaging 2002;29:1039–1046
12. Wester HJ, Herz M, Weber W, Heiss P, Senekowitsch-Schmidtke R, Schwaiger M, et al. Synthesis and radiopharmacology of *O*-(2-[^{18}F]fluoroethyl)-L-tyrosine for tumor imaging. J Nucl Med 1999;40:205–212
13. Heiss P, Mayer S, Herz M, Wester HJ, Schwaiger M, Senekowitsch-Schmidtke R. Investigation of transport mechanism and uptake kinetics of *O*-(2-[^{18}F]fluoroethyl)-L-tyrosine in vitro and in vivo. J Nucl Med 1999;40:1367–1373
14. Langen KJ, Jarosch M, Muhlensiepen H, Hamacher K, Broer S, Jansen P, et al. Comparison of fluorotyrosines and methionine uptake in F98 rat gliomas. Nucl Med Biol 2003;30:501–508
15. Baum RP, Calcagni M, Dimitrakopoulou-Strauss A, Strauss LG. Pharmakokinetic analysis of *O*-2-[^{18}F] fluorethyl-L-tyrosin (^{18}F-FET) by dynamic PET in the differential diagnosis of malignant gliomas. J Nucl Med 2003; 44(Suppl):63P
16. Popperl G, Gotz C, Rachinger W, Gildehaus FJ, Tonn JC, Tatsch K. Value of *O*-(2-[^{18}F]fluoroethyl)-L-tyrosine PET for the diagnosis of recurrent glioma. Eur J Nucl Med Mol Imaging 2004;31:1464–1470
17. Weckesser M, Langen KJ, Rickert CH, Kloska S, Straeter R, Hamacher K, et al. *O*-(2-[^{18}F]fluorethyl)-L-tyrosine PET in the clinical evaluation of primary brain tumours. Eur J Nucl Med Mol Imaging 2005;32:422–429
18. Floeth FW, Pauleit D, Wittsack HJ, Langen KJ, Reifenberger G, Hamacher K, et al Multimodal metabolic imaging of cerebral gliomas: positron emission tomography with [^{18}F]fluoroethyl-L-tyrosine and magnetic resonance spectroscopy. J Neurosurg 2005;102:318–327
19. Kracht LW, Friese M, Herholz K, Schroeder R, Bauer B, Jacobs A, et al. Methyl-[^{11}C]-L-methionine uptake as measured by positron emission tomography correlates to microvessel density in patients with glioma. Eur J Nucl Med Mol Imaging 2003;30:868–873
20. Hernandez-Alcoceba R, Saniger L, Campos J, Nunez MC, Khaless F, Gallo MA, et al. Choline kinase inhibitors as a novel approach for antiproliferative drug design. Oncogene 1997;15:2289–2301
21. Haeffner EW. Studies on choline permeation through the plasma membrane and its incorporation into phosphatidyl choline of Ehrlich-Lettre-ascites tumor cells in vitro. Eur J Biochem 1975;51:219–228
22. Katz-Brull R, Degani H. Kinetics of choline transport and phosphorylation in human breast cancer cells; NMR application of the zero trans method. Anticancer Res 1996;16:1375–1380
23. Yoshimoto M, Waki A, Obata A, Furukawa T, Yonekura Y, Fujibayashi Y. Radiolabeled choline as a proliferation marker: comparison with radiolabeled acetate. Nucl Med Biol 2004;31:859–865
24. Henriksen G, Herz M, Hauser A, Schwaiger M, Wester HJ. Synthesis and preclinical evaluation of the choline transport tracer deshydroxy-[^{18}F]fluorocholine ([^{18}F]dOC). Nucl Med Biol 2004;31:851–858
25. Hara T, Inagaki K, Kosaka N, Morita T Sensitive detection of mediastinal lymph node metastasis of lung cancer with ^{11}C-choline PET. J Nucl Med 2000;41:1507–1513
26. Hara T, Kosaka N, Kishi H. PET imaging of prostate cancer using carbon-11-choline. J Nucl Med 1998;39:990–995
27. Hara T, Kosaka N, Shinoura N, Kondo T PET imaging of brain tumor with [methyl-^{11}C]choline. J Nucl Med 1997;38:842–847
28. Kobori O, Kirihara Y, Kosaka N, Hara T. Positron emission tomography of esophageal carcinoma using ^{11}C-choline and ^{18}F-fluorodeoxyglucose: a novel method of preoperative lymph node staging. Cancer 1999;86:1638–1648
29. Shinoura N, Nishijima M, Hara T, Haisa T, Yamamoto H, Fujii K, et al. Brain tumors: detection with C-11 choline PET. Radiology 1997;202:497–503
30. DeGrado TR, Baldwin SW, Wang S, Orr MD, Liao RP, Friedman HS, et al. Synthesis and evaluation of ^{18}F-labeled choline analogs as oncologic PET tracers. J Nucl Med 2001;42:1805–1814
31. Spaeth N, Wyss MT, Weber B, Scheidegger S, Lutz A, Verwey J, et al. Uptake of ^{18}F-fluorocholine, ^{18}F-fluoroethyl-L-tyrosine, and ^{18}F-FDG in acute cerebral radiation injury in the rat: implications for separation of radiation necrosis from tumor recurrence. J Nucl Med 2004;45:1931–1938
32. Ambar BB, Frei K, Malipiero U, Morelli AE, Castro MG, Lowenstein PR, et al. Treatment of experimental glioma by administration of adenoviral vectors expressing Fas ligand. Hum Gene Ther 1999;10:1641–1648
33. DeGrado TR, Coleman RE, Wang S, Baldwin SW, Orr MD, Robertson CN, et al. Synthesis and evaluation of ^{18}F-labeled choline as an oncologic tracer for positron emission tomography: initial findings in prostate cancer. Cancer Res 2001; 61:110–117
34. Huang SC, Phelps ME, Hoffman EJ, Sideris K, Selin CJ, Kuhl DE. Noninvasive determination of local cerebral metabolic rate of glucose in man. Am J Physiol 1980;238:E69–E82
35. Mikolajczyk K, Szabatin M, Rudnicki P, Grodzki M, Burger C. A JAVA environment for medical image data analysis: initial application for brain PET quantitation. Med Inform (Lond) 1998;23:207–214
36. Saria A, Lundberg JM. Evans blue fluorescence: quantitative and morphological evaluation of vascular permeability in animal tissues. J Neurosci Methods 1983;8:41–49
37. Weidner N, Semple JP, Welch WR, Folkman J. Tumor angiogenesis and metastasis—correlation in invasive breast carcinoma. N Engl J Med 1991;324:1–8
38. Barth RF. Rat brain tumor models in experimental neuro-oncology: the 9L, C6, T9, F98, RG2 (D74), RT-2 and CNS-1 gliomas. J Neurooncol 1998;36:91–102
39. Hustinx R, Smith RJ, Benard F, Bhatnagar A, Alavi A. Can the standardized uptake value characterize primary brain tumors on FDG-PET? Eur J Nucl Med 1999;26:1501–1509
40. Pauleit D, Stoffels G, Schaden W, Hamacher K, Bauer D, Tellmann L, et al. PET with *O*-(2-^{18}F-fluoroethyl)-L-tyrosine in peripheral tumors: first clinical results. J Nucl Med 2005; 46:411–416
41. Shinoura N, Nishijima M, Hara T, Haisa T, Yamamoto H, Fujii K, et al. Brain tumors: detection with C-11 choline PET. Radiology 1997;202:497–503

42. Allen DD, Smith QR. Characterization of the blood-brain barrier choline transporter using the in situ rat brain perfusion technique. J Neurochem 2001;76:1032–1041
43. de Molina AR, Banez-Coronel M, Gutierrez R, Rodriguez-Gonzalez A, Olmeda D, Megias D, et al. Choline kinase activation is a critical requirement for the proliferation of primary human mammary epithelial cells and breast tumor progression. Cancer Res 2004;64:6732–6739
44. Aronen HJ, Pardo FS, Kennedy DN, Belliveau JW, Packard SD, Hsu DW, et al. High microvascular blood volume is associated with high glucose uptake and tumor angiogenesis in human gliomas. Clin Cancer Res 2000;6:2189–2200
45. Leon SP, Folkerth RD, Black PM. Microvessel density is a prognostic indicator for patients with astroglial brain tumors. Cancer 1996;77:362–372
46. Kaschten B, Stevenaert A, Sadzot B, Deprez M, Degueldre C, Del Fiore G, et al. Preoperative evaluation of 54 gliomas by PET with fluorine-18-fluorodeoxyglucose and/or carbon-11-methionine. J Nucl Med 1998;39:778–785
47. Padma MV, Said S, Jacobs M, Hwang DR, Dunigan K, Satter M, et al. Prediction of pathology and survival by FDG PET in gliomas. J Neurooncol 2003;64:227–237
48. Cheon GJ, Ahn SH, Cho YS, Kwack HS, Lee CH, Choi CW, et al. Correlation of ^{18}F-FET uptake and histologic grades of primary brain tumors. J Nucl Med 2003;44 Suppl:367P
49. Pauleit D, Floeth F, Hamacher K, Riemenschneider MJ, Reifenberger G, Muller HW, et al. *O*-(2-[^{18}F]fluoroethyl)-L-tyrosine PET combined with MRI improves the diagnostic assessment of cerebral gliomas. Brain 2005;128:678–687
50. Pauleit D, Floeth F, Tellmann L, Hamacher K, Hautzel H, Muller HW, et al. Comparison of *O*-(2-^{18}F-fluoroethyl)-L-tyrosine PET and 3-^{123}I-iodo-alpha-methyl-L-tyrosine SPECT in brain tumors. J Nucl Med 2004;45:374–381
51. Tian M, Zhang H, Higuchi T, Oriuchi N, Endo K. Oncological diagnosis using ^{11}C-choline-positron emission tomography in comparison with 2-deoxy-2-[^{18}F]fluoro-D-glucose-positron emission tomography. Mol Imaging Biol 2004;6:172–179
52. Tian M, Zhang H, Oriuchi N, Higuchi T, Endo K. Comparison of ^{11}C-choline PET and FDG PET for the differential diagnosis of malignant tumors. Eur J Nucl Med Mol Imaging 2004; 31:1064–1072
53. Utriainen M, Komu M, Vuorinen V, Lehikoinen P, Sonninen P, Kurki T, et al. Evaluation of brain tumor metabolism with [^{11}C] choline PET and ^{1}H-MRS. J Neurooncol 2003;62:329–338